A Closed-Form Approximation of the Gaussian Noise Model in the Presence of Inter-Channel Stimulated Raman Scattering

Daniel Semrau 🅾, *Student Member, IEEE*, Robert I. Killey, *Senior Member, IEEE*,
and Polina Bayvel, *Fellow, IEEE, Fellow, OSA*

Abstract—An accurate, closed-form expression evaluating the nonlinear interference (NLI) power in coherent optical transmission systems in the presence of inter-channel stimulated Raman scattering (ISRS) is derived. The analytical result enables a rapid estimate of the signal-to-noise ratio and avoids the need for integral evaluations and split-step simulations. The formula also provides a new insight into the underlying parameter dependence of ISRS on the NLI. Additionally, it accounts for the dispersion slope and arbitrary launch power distributions including variably loaded fiber spans. The latter enables real-time modeling of optical mesh networks. The results is applicable for lumped amplified, dispersion unmanaged, and ultra-wideband transmission systems. The accuracy of the closed-form expression is compared to numerical integration of the ISRS Gaussian noise model and split-step simulations in a point-to-point transmission, as well as in a mesh optical network scenario.

Index Terms—C+L band transmission, closed-form approximation, first-order perturbation, Gaussian noise model, nonlinear interference, nonlinear distortion, optical fiber communications, stimulated Raman scattering.

I. INTRODUCTION

ANALYTICAL models to estimate nonlinear interference (NLI) are key for rapid and efficient system design [1], achievable rate estimations of point-to-point links [2]–[4] and physical layer aware network optimization. The latter is essential for optical network abstraction and virtualization leading to optimal and intelligent techniques to maximize optical network capacity [5].

Most approaches analytically solve the nonlinear Schrödinger equation using first-order perturbation theory with respect to the Kerr nonlinearity. The resulting integral expressions offer a significant reduction in computational complexity with minor in-
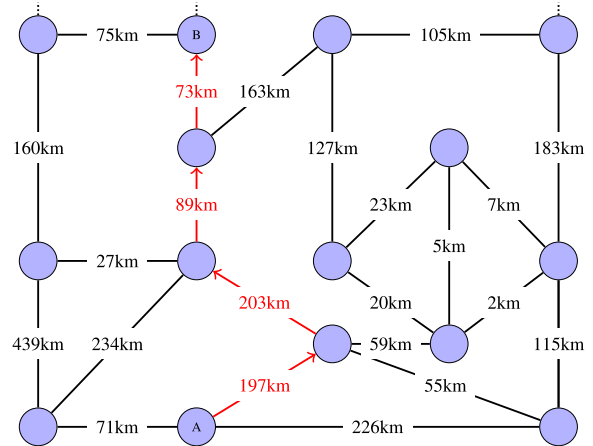
Fig. 1. A section from the British Telecommunications (BT) 20+2 topology of the United Kingdom (UK) core network [16]. In section III-D, the nonlinear interference of the example light path (A-B) is modeled.

accuracies, compared to split-step simulations and experiments [6]–[11].

In particular, the Gaussian Noise (GN) model offers a reasonable accuracy with moderate computational complexity [12], [13]. Numerical integration of the GN model to obtain the nonlinear interference has a typical computation time of a few minutes per WDM channel [14], [15]. For ultra-wideband signals with over 200 WDM channels, the computation time quickly increases to a few hours to obtain the NLI distribution across the entire optical bandwidth.

For some applications, such time frames are not acceptable and closed-form approximations, that yield performance estimations in picoseconds, are required. Such applications include e.g. physical layer aware network optimization and network performance estimation. In addition to speed, closed-form approximations offer a unique insight into the underlying parameter dependencies and provide useful design and scaling rules.

An optical mesh network consists of a large number of point-to-point links, carrying many lightpaths. As an example, the British Telecommunications (BT) 20+2 topology of the United Kingdom core network [16] has 34 bidirectional network edges. A section of the network is shown in Fig. 1. Assuming a WDM grid spacing of 50 GHz (ITU grid) over the entire C+L band (10 THz), a full performance estimation of a *single* network state

requires up to $\frac{10\,\text{THz}}{50\,\text{GHz}} \cdot 2 \cdot 34 = 13600$ performance evaluations. It is evident that the problem is intractable using numerical integration. However, using closed-form approximations, the performance estimation of an entire network state can be reduced to only a few microseconds.

Closed-form approximations, that predict the nonlinear interference power in coherent transmission systems, were derived for lossless fibers [3], [17] and lossy fibers using lumped amplification [13], [18]–[22] as well as distributed Raman amplified links [23].

However, all aforementioned formulas are not applicable for optical bandwidths beyond C-band (5 THz) where inter-channel stimulated Raman scattering (ISRS) becomes significant. ISRS is a non-parametric nonlinear effect that effectively amplifies low frequency components at the expense of high frequency components within the same optical signal. This significantly alters the NLI distribution across the received spectrum.

A GN model that accounts for ISRS, in integral and in closed-form, was first proposed in our previous work [24]. The effect of ISRS was included through a channel dependent exponential decay, valid in the weak ISRS regime. A more generalized model, in integral form, termed ISRS GN model, was subsequently proposed in [14], [15], [25]–[27]. The ISRS GN model accurately accounts for strong ISRS power transfers, as well as for distributed amplification techniques. A more detailed comparison can be found in [27] and experimental validations can be found in [11], [26]. However, the ISRS GN model relies on numerically solving an integral of at least three dimensions and an approximation in closed-form has not been reported to date.

In this paper, a closed-form approximation of the ISRS GN model is presented which accurately accounts for the impact of ISRS on the nonlinear interference power. The derived formula generalizes our previous results in [24] by including the dispersion slope, the improved ISRS description of the ISRS GN model and arbitrary launch power distributions, including variably loaded fiber spans. The latter enables real time performance estimations in optical mesh networks. The proposed formula is applicable to dispersion unmanaged ultra-wideband transmission systems with lumped amplifiers. The formula is validated by split-step simulations over 10.05 THz optical bandwidth.[1]

The remainder of this paper is organized as follows: The ISRS GN model is briefly summarised in Section II-A. Section II-B addresses the key steps in the derivation of the closed-form approximation and the result is presented in Section II-C. In Section III, the proposed formula is validated via split-step simulations and via the ISRS GN model in integral form for a point-to-point transmission and a mesh network scenario. Section IV addresses the case of non-uniform (tilted) launch power distributions.

---

[1]Simultaneously with this submission here, this paper was submitted to arXiv e-prints [28]. During the peer-review process, [29] appeared on arXiv. The approach in [29] is very similar to the one presented here. Comparison of the results for the parameters used in Fig 5 in this manuscript, yield an average difference of less than 0.1 dB.

II. THE ISRS GN MODEL IN CLOSED-FORM

In this section, the proposed closed-form approximation of the ISRS GN model is presented. The main derivation steps are outlined and its key assumptions are addressed and discussed.

After coherent detection, electronic dispersion compensation and neglecting the impact of transceiver noise, the signal-to-noise ratio (SNR) of the channel of interest (COI) i can be calculated as

$$\text{SNR}_i \approx \frac{P_i}{P_{\text{ASE}} + \eta_n P_i^3}, \qquad (1)$$

where P_i is the launch power of channel i at the transmitter and P_{ASE} is the accumulated amplified spontaneous emission (ASE) noise originating from optical amplifiers. ASE noise inflation as a result of gain equalization can be included by a channel dependent P_{ASE}. The nonlinear interference coefficient $\eta_n (f_i)$ after n spans is dependent on the center frequency f_i of the COI.

For optical bandwidths beyond C-band (5 THz), inter-channel stimulated Raman scattering becomes significant. ISRS leads to a power transfer of an incident pump wave to lower frequency (Stokes) waves through the intermediary of optical lattice vibrations in the guiding medium. The probability of this power transfer is enhanced with increasing frequency separation between pump and Stokes wave according to the Raman gain function [30]. In the context of perturbation based models, the impact of ISRS on the Kerr effect is modeled by changing the effective attenuation (the signal power profile) across the transmitted spectrum to resemble the average effect of ISRS, neglecting temporal fluctuations. To this date, all approaches available in the literature treat transmitted channels as continuous waves and hence neglect temporal gain fluctuations resulting from channel modulation. The negligible nature of such dynamic effects is motivated by the averaging of many independent sources which has been theoretically shown for on-off keyed systems [31], [32]. Recently, this has been experimentally demonstrated over continuous bandwidths of 3 THz [26] and 9 THz [11] and between the S- and L-band [33].

A. The ISRS GN Model in Integral Form

In the following the ISRS GN model, a Gaussian model that accounts for inter-channel stimulated Raman scattering, is briefly revised.

The NLI coefficient in the presence of ISRS is given by [27, Eq. (9)]

$$\eta_1 (f_i) = \frac{B_i}{P_i^3} \frac{16}{27} \gamma^2 \int df_1 \int df_2 \, G_{\text{Tx}}(f_1) G_{\text{Tx}}(f_2)$$

$$\cdot G_{\text{Tx}}(f_1 + f_2 - f_i)$$

$$\cdot \left| \int_0^L d\zeta \, \frac{P_{\text{tot}} e^{-\alpha\zeta - P_{\text{tot}} C_r L_{\text{eff}} \cdot (f_1 + f_2 - f_i)}}{\int G_{\text{Tx}}(\nu) e^{-P_{\text{tot}} C_r L_{\text{eff}} \nu} d\nu} e^{j\phi(f_1, f_2, f_i, \zeta)} \right|^2, \quad (2)$$

where B_i is the bandwidth of the COI i, γ is the nonlinearity coefficient, α is the attenuation coefficient, $L_{\text{eff}} = \frac{1 - e^{-\alpha\zeta}}{\alpha}$ (the ζ dependence is suppressed throughout this paper for notational brevity), C_r is the slope of the linear regression of the normalized Raman gain spectrum, P_{tot} is the total transmitted optical
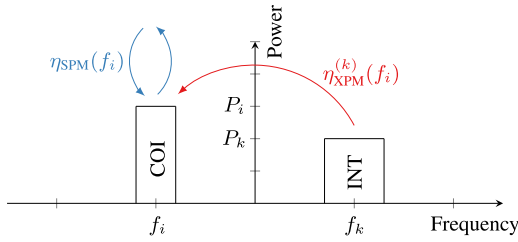
Fig. 2.   Illustration of the transmitted spectrum $G_{\mathrm{Tx}}(f)$ subject to the XPM assumption. Shown are the channel under test (COI) and a single interferer (INT) with arbitrary power levels, bandwidths and center frequencies. The total XPM is then obtained by summing over all interferers $k \in S_i$ as in (4).

power and $\phi = -4\pi^2 (f_1 - f_i)(f_2 - f_i)\left[\beta_2 + \pi\beta_3(f_1 + f_2)\right]\zeta$ is a phase mismatch term, with the group velocity dispersion (GVD) parameter β_2 and its linear slope β_3 at the reference wavelength.

Eq. (3) is valid for optical bandwidths of up to 15 THz as it assumed a linear (rectangular) Raman gain spectrum. The ISRS GN model in integral form for multi-span systems (where different spans exhibit different launch power distributions) can be found in [14, Eq. (2)]. Eq. (3) assumes a uniform NLI power spectral density (PSD) over the channel bandwidth (the local white noise assumption). This assumption is required in order to avoid the integration of the NLI PSD over the receiver (matched) filter, which is analytically difficult for arbitrary filter shapes.

The strength of ISRS for a given system can be assessed by calculating the net power transfer $\Delta\rho(z)$ between the outer channels of the WDM signal. This is the summation of the ISRS net gain/loss of the highest and lowest frequency channel, which is given by [34], [35]

$$\Delta\rho(z)\,[\mathrm{dB}] \triangleq 10\log_{10}\left[\Delta\rho(z)\right] = 4.3 \cdot P_{\mathrm{tot}} C_{\mathrm{r}} L_{\mathrm{eff}} B_{\mathrm{tot}}, \quad (3)$$

where B_{tot} is the total optical bandwidth.

B. The XPM Assumption

In the following, some of the key steps in deriving the proposed closed-form approximation of (3) are addressed and discussed.

We first evaluate the nonlinear perturbation of the COI i, caused by a single interferer (INT) k, which is denoted by $\eta_{\mathrm{XPM}}^{(k)}(f_i)$. The special case where the NLI is caused by the COI itself (i.e. $k = i$), is denoted by SPM (also denoted by SCI). The NLI contribution of all other interferers is denoted as XPM (also denoted by XCI). An illustration of the SPM and XPM contribution of a COI and a single INT is schematically shown in Fig. 2. In more detail, the set of all XPM interferers, with respect to the COI i, is given as

$$S_i = \{k \in \mathbb{N}\,|\,1 \le k \le N_{\mathrm{ch}} \text{ and } k \ne i\}. \quad (4)$$

In the literature, this assumption is often referred to as XPM assumption [21], [36]–[39] and it neglects NLI contributions that are jointly generated by two interfering channels, which is denoted as FWM (also denoted by MCI). However, this contribution is typically very small in highly dispersive links, where high symbol rates or channel spacings are used [40], [41].

Using the XPM assumption, the NLI coefficient is

$$\eta_n(f_i) \approx \sum_{j=1}^{n}\left[\frac{P_{i,j}}{P_i}\right]^2 \cdot \left[\eta_{\mathrm{SPM,j}}(f_i)\,n^\epsilon + \eta_{\mathrm{XPM,j}}(f_i)\right], \quad (5)$$

where $\eta_{\mathrm{SPM,j}}(f_i)$ is the SPM contribution and $\eta_{\mathrm{XPM,j}}(f_i)$ is the total XPM contribution generated in the j'th span. $P_{i,j}$ is the power of channel i launched into the j'th span, where $P_{i,1} = P_i$. Eq. (5) essentially returns the NLI coefficient of each span, normalized to the launch power of the transmitter. Different launch power distributions and fiber parameters for each span can be accounted for. However, for the remainder of this paper, the j dependence of the SPM and XPM contribution is suppressed for notational convenience.

The total XPM contribution is obtained by summing over all interfering channels, as

$$\eta_{\mathrm{XPM}}(f_i) = \sum_{\forall k \in S_i} \eta_{\mathrm{XPM}}^{(k)}(f_i), \quad (6)$$

where $\eta_{\mathrm{XPM}}^{(k)}(f_i)$ is the XPM contribution of a single interfering channel k on channel i.

The coherent accumulation along multiple fiber spans is included using the coherence factor ϵ. The coherence factor can be obtained in closed-form [13, Eq. (22)]. The coherence factor is typically defined for the entire optical signal. However in this work, only the SPM contribution is assumed to accumulate coherently and the coherence factor is redefined over the channel bandwidth B_i [42]. The XPM contribution is assumed to accumulate incoherently. The advantage of this approach is that the coherent accumulation is independent of the transmitted spectrum and is only a function of the channel bandwidth. This significantly simplifies the modeling of NLI in optical mesh networks as fiber spans are variably loaded. The approach is consistent with the observations in [40].

Additionally, it is assumed that the coherence factor itself is not altered by ISRS, which is not strictly true as shown in [27]. However, this effect is neglected due to its small impact on the NLI. For SSMF based spans and a 10 THz signal, this results in an approximation error of around 0.1 dB after 10 fiber spans.

In the following, the NLI caused by a single interferer on the COI, is analytically evaluated. It is assumed that the channel of interest i has normalized pulse shape $g_i(f - f_i) = \frac{1}{B_i}\Pi\left(\frac{f - f_i}{B_i}\right)$, launch power P_i, channel bandwidth B_i and is centered around frequency f_i. The function $\Pi(x)$ denotes the rectangular function. The interfering channel has normalized pulse shape $g_k(f - f_k) = \frac{1}{B_k}\Pi\left(\frac{f - f_k}{B_k}\right)$, launch power P_k, bandwidth B_k and is centered around frequency f_k. The transmitted spectrum is then given by

$$G_{\mathrm{Tx}}(f) = P_i g_i(f - f_i) + P_k g_k(f - f_i - \Delta f), \quad (7)$$

where $\Delta f = f_k - f_i$ is the frequency separation between COI and INT. An illustration of (7) with the resulting nonlinear interactions on the COI is shown in Fig. 2.

Substituting the transmitted spectrum (7) in the ISRS GN model (3) yields six non-identical terms where only two are non-zero and contribute to the NLI of the COI. These two terms

are the SPM and the XPM contribution. The XPM contribution is

$$\eta_{\text{XPM}}^{(k)}(f_i) = \frac{32}{27} \frac{\gamma^2}{B_k^2} \left(\frac{P_k}{P_i} \right)^2 \int_{-\frac{B_i}{2}}^{\frac{B_i}{2}} df_1 \int_{-\frac{B_k}{2}}^{\frac{B_k}{2}} df_2 \, \Pi \left(\frac{f_1 + f_2}{B_k} \right)$$

$$\cdot \left| \int_0^L d\zeta \, \frac{P_{\text{tot}} e^{-\alpha\zeta - P_{\text{tot}} C_r L_{\text{eff}} \cdot (f_1 + f_2 + f_k)}}{\int G_{\text{Tx}}(\nu) e^{-P_{\text{tot}} C_r L_{\text{eff}} \nu} d\nu} e^{j\phi(f_1 + f_i, f_2 + f_k, f_i, \zeta)} \right|^2, \tag{8}$$

and the SPM contribution is

$$\eta_{\text{SPM}}(f_i) = \frac{1}{2} \eta_{\text{XPM}}^{(i)}(f_i). \tag{9}$$

It should be noted that in Eq. (9) P_{tot}, B_{tot} and $G_{\text{Tx}}(\nu)$ refer to the launch power, bandwidth and transmitted spectrum of the *entire* WDM signal.

C. The ISRS GN Model in Closed-Form

The SPM and the XPM contributions are solved separately yielding two formulas, one for each contribution. The total NLI is then obtained using (5). The reader is referred to Appendix A and Appendix B for the detailed derivations.[2]

The closed-form approximation for the SPM contribution is

$$\eta_{\text{SPM}}(f_i) \approx \frac{4}{9} \frac{\gamma^2}{B_i^2} \frac{\pi}{\phi_i \bar{\alpha} (2\alpha + \bar{\alpha})}$$

$$\cdot \left[\frac{T_i - \alpha^2}{a} \text{asinh} \left(\frac{\phi_i B_i^2}{\pi a} \right) + \frac{A^2 - T_i}{A} \text{asinh} \left(\frac{\phi_i B_i^2}{\pi A} \right) \right], \tag{10}$$

with $\phi_i = \frac{3}{2}\pi^2 (\beta_2 + 2\pi\beta_3 f_i)$, $A = \alpha + \bar{\alpha}$ and $T_i = (\alpha + \bar{\alpha} - P_{\text{tot}} C_r f_i)^2$.

The closed-form approximation for the total XPM contribution is

$$\eta_{\text{XPM}}(f_i) \approx \frac{32}{27} \sum_{k=1, k \neq i}^{N_{\text{ch}}} \left(\frac{P_k}{P_i} \right)^2 \frac{\gamma^2}{B_k \phi_{i,k} \bar{\alpha} (2\alpha + \bar{\alpha})}$$

$$\cdot \left[\frac{T_k - \alpha^2}{\alpha} \text{atan} \left(\frac{\phi_{i,k} B_i}{\alpha} \right) + \frac{A^2 - T_k}{A} \text{atan} \left(\frac{\phi_{i,k} B_i}{A} \right) \right], \tag{11}$$

with $\phi_{i,k} = 2\pi^2 (f_k - f_i) [\beta_2 + \pi\beta_3 (f_i + f_k)]$. The sum in (11) represents the summation over the XPM contribution of each individual interferer as in (4).

If not specified otherwise, it holds that $\bar{\alpha} = \alpha$. The parameter $\bar{\alpha}$ can be used to apply the proposed closed-formula in more general cases. Such cases include improved accuracy for non-uniform (tilted) launch power distributions, wavelength dependent attenuation and even the extension of the formula beyond 15 THz i.e. beyond the triangular region of the Raman gain spectrum. This is done by reinterpreting α, $\bar{\alpha}$ and C_r as channel *dependent* quantities. The parameters are then matched to reproduce the actual power profile of each channel and the proposed formula can be applied. The drawback of this strategy is

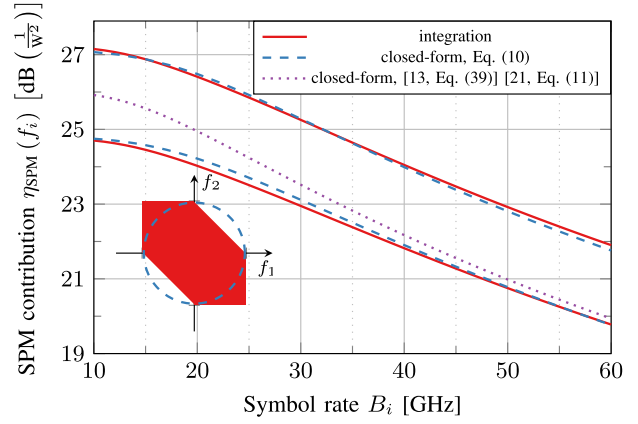[2]An implmentation in MATLAB and Python can be found at [43].

Fig. 3. SPM contribution for $i = 25$ with $f_i = -4040$ GHz as a function of symbol rate (bandwidth), obtained from numerically solving the ISRS GN model in integral form (8) and its proposed approximation in closed-form (10). The inset shows the actual integration domain and its circular approximation. For comparison the results of [13] [21] are shown, which both model SPM in the absence of ISRS.
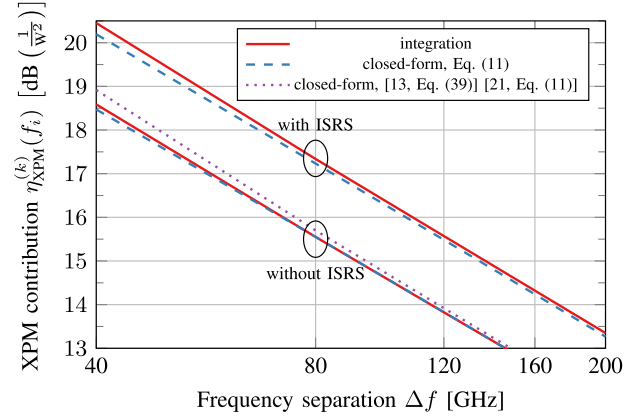

Fig. 4. XPM contribution for $i = 25$ with $f_i = -4040$ GHz as a function of frequency separation between channel of interest (COI) and interferer (INT), obtained from numerically solving the ISRS GN model in integral form (8) and its proposed approximation in closed-form (11), for $k \in \{26, 27, 28, 29, 30\}$. For comparison the results of [13] [21] are shown, which both model XPM in the absence of ISRS.

larger complexity as the Raman equations must be solved numerically and additional regression operations are necessary in order to obtain the channel dependent α, $\bar{\alpha}$ and C_r. The case of non-uniform (tilted) launch power distributions is addressed in Sec. IV. The other cases are the subject of future publications.

D. Convergence to Previously Reported Results in the Absence of ISRS

The SPM contribution as a function of symbol rate (channel bandwidth) is shown in Fig. 3 and the XPM contribution as a function of channel separation is shown in Fig. 4. The results were obtained by numerically integrating (8) and its proposed approximation in closed-form. A WDM signal with an optical bandwidth of 10.05 THz was assumed with a channel launch power of 0 dBm. The COI has a center frequency of

TABLE I
SYSTEM PARAMETERS

Parameters	
Loss (α) [dB/km]	0.2
Dispersion (D) [ps/nm/km]	17.0
Dispersion slope (S) [ps/nm²/km]	0.067
NL coefficient (γ) [1/W/km]	1.2
Raman gain slope (C_r) [1/W/km/THz]	0.028
Raman gain ($C_r \cdot 14$ THz) [1/W/km]	0.4
Symbol rate [GBd]	40
Channel Bandwidth (B_i) [GHz]	40.004
Channel Launch Power (P_i) [dBm]	0
Total Launch Power (P_{tot}) [dBm]	24
Channel spacing [GHz]	40.005
Number of channels	251
Optical bandwidth (B_{tot}) [THz]	10.05
Reference Wavelength [nm]	1550
Roll-off factor [%]	0.01
Number of symbols [2^x]	17
Simulation steps per span [10^6]	0.25 to 1

$f_i = -4040$ GHz and is transmitted with a single interferer over 100 km SMF with parameters listed in Table I . The accuracy of the closed-form approximation is remarkable throughout Figs. 3 and 4, with an average deviation of < 0.1 dB and 0.1 dB without and with ISRS, respectively.

In the absence of ISRS, the proposed formula is comparable to the formulas proposed in [13, Eq. (39)] [21, Eq. (11)]. Both are shown in Figs. 3 and 4, where the dispersion slope was included for a fair comparison. Without ISRS, both formulas are very close to the result proposed in this work, except for lower symbol rates. For the SPM contribution, this difference mainly originates in the assumed integration domain. The proposed formula assumes a circular integration domain, whereas [13, Eq. (39)] [21, Eq. (11)] both assume a rectangular integration domain. A circular integration domain provides better accuracy for lower symbol rates and yields analytical solutions in terms of elementary functions as opposed to special functions [20].

E. Discussion of Key Assumptions

The closed-form formulas (10) and (11) were derived from the ISRS GN model in integral form (8) with three key assumptions:

Assumption 1: For the XPM contribution, the frequency separation between the channel of interest and the interfering channel is much greater than half of the channel bandwidth, i.e. $|\Delta f| \gg \frac{B_k}{2}$.

Assumption 2: The impact of ISRS on the effective channel power attenuation (the signal power profile) is small, which means that it can be approximated by a first-order Taylor series.

Assumption 3: The effective channel power attenuation is only a function of the total launch power and independent of its spectral distribution. This assumption has no impact on a uniform launch power distribution.

Assumption 1 is mathematically equivalent with the zeroth-order solution of the inner integral, over f_2, in Eq. (8). In Appendix C, it is shown that the introduced relative approximation error of the XPM conribution is upper bounded by

$$\text{Rel. Err.} < 8\% \cdot \left(\frac{B_k}{\Delta f}\right)^2 . \tag{12}$$

For the closest channel spacing with $\Delta f = (k - i) \cdot B_k$, assumption 1) introduces an approximation error of *at most* 0.3 dB for a directly adjacent channel and approximation errors of <0.1 dB for all other interfering channels. The analysis explains the excellent match between closed-form and integral evaluation in Fig. 4. As the *total* XPM power is a summation over numerous interfering channels, the approximation error of assumption 1) can be deemed negligible.

Assumption 2 holds when the impact of ISRS on the the effective channel power attenuation (the signal power profile) can be considered low. Mathematically, the ISRS term is approximated by a first-order Taylor series. A validity range can be derived by analyzing higher order terms. In particular, we compare the first-order and second-order terms of the Taylor expansion used to approximate ISRS. The reader is referred to Appendix D for a detailed derivation. It is found that the second-order term is negligible if

$$0.23 \cdot \Delta \rho\,(L)\,[\text{dB}] \ll 6. \tag{13}$$

The power transfer between the outer channels of the assumed WDM signal in Figs. 3 and 4 is $\Delta \rho\,(L)\,[\text{dB}] = 6.3$ dB and the particular ISRS gain of the CUT is 2.3 dB. Eq. (13) yields $1.4 \ll 6$ which is not fully satisfied. This results in a small approximation error in the presence of ISRS.

Assumption 3 introduces no approximation error when the launch power distribution is uniform. In general, ISRS changes the effective attenuation for a given WDM channel during propagation. This change is a function of the total transmitted launch power, mathematically expressed as $e^{-P_{tot}C_r L_{eff}(f_1 + f_2 - f_i)}$ in (3), and its spectral distribution, mathematically expressed as $\frac{1}{P_{tot}} \int G_{Tx}(\nu)e^{-P_{tot}C_r L_{eff}\nu} d\nu$ in (3). In deriving the proposed closed-form formula, it was assumed that (for the ISRS term) the total optical launch power is uniformly distributed over the entire optical bandwidth. This effectively assumes that the effective channel power attenuation (the signal power profile) is *independent* of the launch power distribution and only dependent on the total launch power. The impact of this assumption is quantified for mesh optical networks in Section III-D and tilted launch power distributions in Section IV.

Additionally, in Section IV, a strategy is proposed to completely eliminate the approximation error of assumption 3) by matching the parameters α, $\bar{\alpha}$ and C_r to the actual power profile present in the fiber span.

III. NUMERICAL VALIDATION

In this section the proposed closed-form approximations (10) and (11) are validated in an optical transmission system with parameters listed in Table I. The validation is performed for a point-to-point transmission in III-C and for a mesh optical network scenario in III-D.

A. Setup

The validation was carried out by numerically solving the Manakov equation using the well established split-step Fourier method (SSFM). Inter-channel stimulated Raman scattering was included in the SSFM by applying a frequency dependent loss
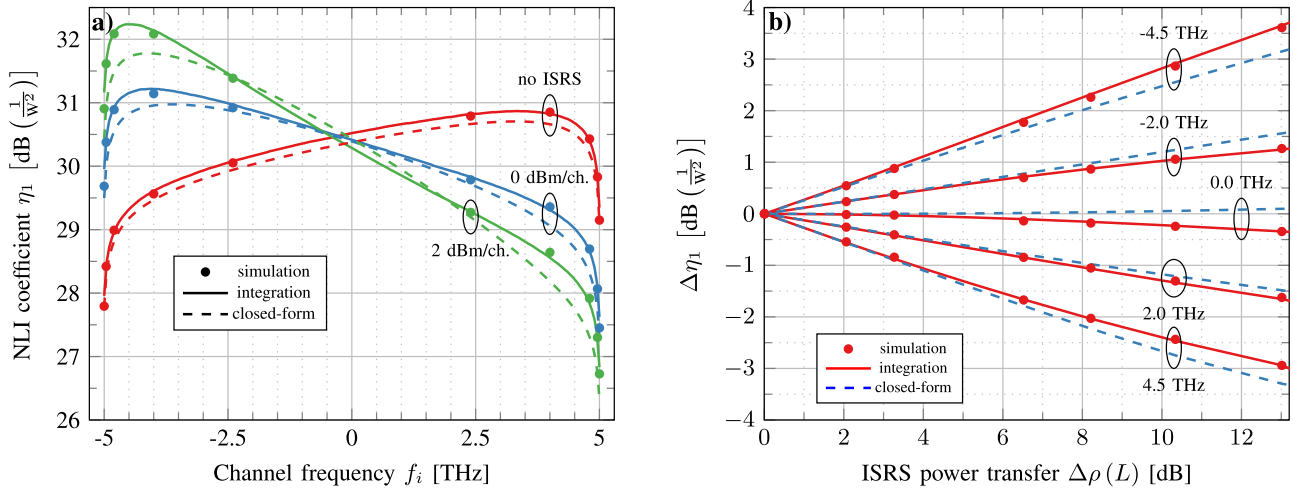
Fig. 5. The NLI coefficient after one 100 km span as a function of channel frequency is shown in (a). The deviation of the NLI coefficient after one span as a function of ISRS power transfer for different channels within the transmitted WDM signal is shown in (b). The results were obtained by numerical simulations, numerically solving the ISRS GN model in integral form (3) and its proposed approximation in closed-form (10) and (11).

at every linear step, so that the signal power profile altered by ISRS, is obtained.

A logarithmic step size distribution was implemented, where $0.25 \cdot 10^6$ simulation steps were found to be sufficient for launch powers as high as 0 dBm per channel and $1 \cdot 10^6$ for launch powers as high as 3 dBm/ch. Launch powers of up to 3 dBm/ch. were considered in order to check the validity of the weak ISRS assumption (see assumption 2 in Section II-E). At the beginning of the fiber, the step size was as short as 21.5 cm, while the step size at the end of a span was 2.15 m for 3 dBm/ch.

Gaussian symbols, drawn from a circular-symmetric Gaussian distribution and uniform 64-QAM symbols were used for transmission. The former was chosen in order to verify the closed-form approximation while the latter was chosen to compare the performance to a standard modulation format.

The receiver consisted of digital dispersion compensation, ideal root-raised-cosine (RCC) matched filtering and constellation rotation. The SNR was ideally estimated as the ratio between the variance of the transmitted symbols $E[|X|^2]$ and the variance of the noise σ^2, where $\sigma^2 = E[|X - Y|^2]$ and Y represents the received symbols after digital signal processing. The nonlinear interference coefficient was then estimated via Eq. (1). In order to improve the simulation accuracy, four different data realizations were simulated and averaged for each transmission.

Ideal, noiseless amplifiers were considered to ease the NLI computation and for a fair comparison between numerical simulation and ISRS GN model.

B. Single Span Transmission

The spectral distribution of the NLI coefficient after a single span obtained by the SSFM, the ISRS GN model in integral form and its proposed approximation in closed form are shown in Fig. 5a. Launch powers of 0 dBm/ch. and 2 dBm/ch. are shown which results in an ISRS power transfer of $\Delta\rho(L)\,[\text{dB}] = 6.3$ dB and $\Delta\rho(L)\,[\text{dB}] = 10.3$ dB, respectively. A case, where no ISRS is considered is shown for comparison.

The tilt in NLI, in the case of no ISRS, is due to the dispersion slope S (or β_3), where low frequency components exhibit a higher amount of dispersion resulting in lower nonlinear penalties. With increasing launch powers, low frequency components are increasingly amplified, at the expense of high frequency components, leading to increased (reduced) NLI for low (high) frequency components.

Not surprisingly, the ISRS GN model in integral form matches the simulation results with negligible error except at the most outer channels due to the local white noise assumption (which could be lifted by properly integrating the NLI PSD over the channel bandwidth). The proposed closed-form approximation is in good agreement with the ISRS GN model in integral form and the simulation results. The average gap, in the case of no ISRS, is 0.1 dB. This discrepancy is due to the XPM assumption (see Section II-B), as the individual SPM and XPM contributions are approximated with negligible error, as shown in Figs. 3 and 4. The average discrepancy is 0.1 dB for 0 dBm/ch. and 0.2 dB for 2 dBm/ch. launch power. The increasing discrepancy with increasing launch power is due to the weak ISRS assumption (see Section II-E). This assumption has more impact on the outer channels as the net ISRS gain is larger.

The deviation of the NLI coefficient as a function of the ISRS power transfer $\Delta\rho(L)\,[\text{dB}]$ for different channels within the WDM signal is shown in Fig. 5 b. The discrepancy between the ISRS GN model in integral form and the SSFM is negligible for the shown range of power transfers. Due to the weak ISRS assumption, the accuracy of the closed-form expression decreases with increasing ISRS. This is because higher order terms of the Taylor expansion are becoming significant.

C. A Point-to-Point Transmission Scenario

In this section, a multi-span transmission system, consisting of six identical 100 km SMF fiber spans, is studied with parameters listed in Table I. A uniform launch power of 0 dBm/ch. was
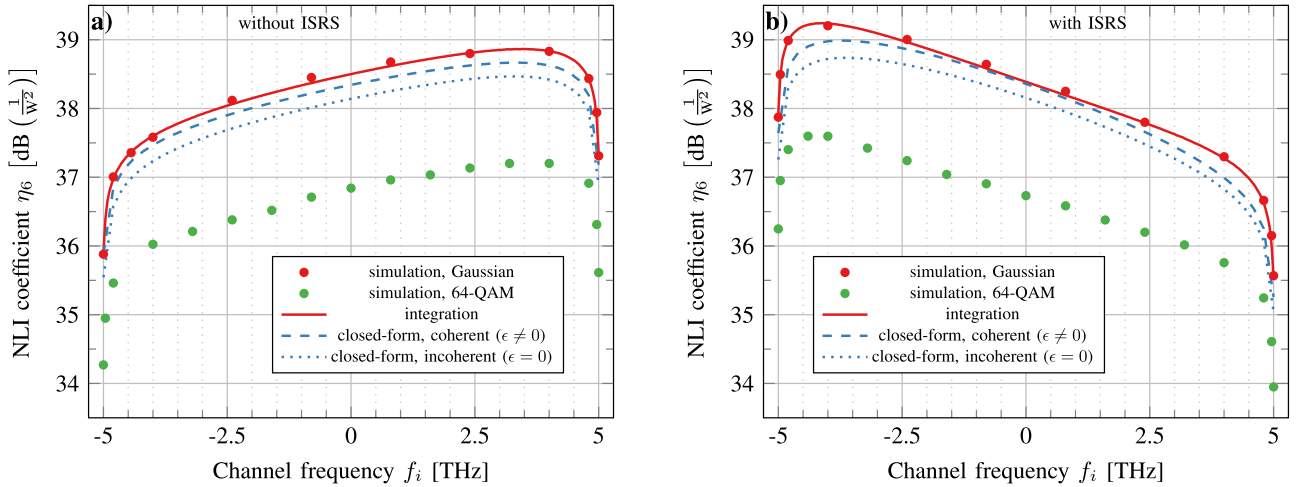
Fig. 6. The distribution of the NLI coefficient after 6 spans (600 km) without a) and with b) ISRS. A launch power of 0 dBm/ch. was considered yielding an ISRS power transfer of $\Delta\rho(L)$ [dB] = 6.3 dB. The results were obtained by numerical simulations, the ISRS GN model in integral form (3) and its proposed approximation in closed-form (10) and (11), in coherent and incoherent form.

used which is the optimum launch power for the central channel in the presence of Erbium-doped fiber amplifiers (EDFA) with a noise figure of 5 dB. The ISRS power transfer was equalized by a gain flattening filter after every fiber span.

The NLI coefficient after six spans is shown in Fig. 6a without accounting for ISRS and in Fig. 6b accounting for ISRS. Simulation results using Gaussian modulation as well as uniform 64-QAM are shown together with the ISRS GN model in integral form and its proposed approximation in closed-form. To account for coherent accumulation and variably loaded fiber spans, the ISRS GN model takes a slightly different form which was published in [14, Eq. (2)] and used to obtain the results in Fig. 6.

The closed-form approximation is considered with an incoherent ($\epsilon = 0$) and a coherent ($\epsilon \neq 0$) accumulation of NLI along multiple fiber spans (5). The coherence factor of the given system configuration is $\epsilon = 0.15$. The average gap between the closed-form, including a coherent accumulation, and the ISRS GN model in integral form is 0.1 dB and 0.2 dB without and with ISRS, respectively. The accuracy is similar to the single span case (see Fig. 5), indicating that Eq. (5) sufficiently approximates the coherent accumulation of NLI.

A majority of the NLI originates from XPM, which is accumulating incoherently. The formalism may therefore be simplified by assuming an incoherent accumulation and setting $\epsilon = 0$. The average accuracy loss, of assuming incoherent accumulation, is 0.2 dB for the studied system. Depending on accuracy requirements, this error may be deemed negligible. It should be noted, however, that this accuracy loss (with respect to Gaussian modulation) increases with the number of spans.

A key assumption of the model is that each frequency component carries a symbol drawn from a symmetric circular Gaussian distribution which leads to an overestimation of the NLI power with respect to square QAM formats. To compare the model predictions to a standard modulation format, the NLI coefficient using 64-QAM obtained by the SSFM is shown in Fig. 6. The

average gap between SSFM using 64-QAM and the closed-form approximation in coherent form is 1.6 dB in both cases, without and with ISRS. This gap decreases with increasing accumulated dispersion, hence, with increasing transmission distance. Additionally, modern transmission systems utilize probabilistic or geometric shaping which further decreases this gap as shaped signals partially resemble Gaussian modulated signals [44], [45].

In summary, the proposed closed-form approximation models the impact of ISRS on the NLI (SPM and XPM) with excellent accuracy in fully occupied point-to-point transmission scenarios. In can, therefore, be used for system design, optimization and real-time performance estimations of ultra-wideband transmission point-to-point links.

D. A Mesh Optical Network Scenario

In this section, the closed-form approximation (10) and (11) is applied and validated in a mesh optical network. The fundamental difference in a mesh network, as opposed to a point-to-point transmission, is that not all channels within a WDM signal are transmitted along the *entire* lightpath. At each reconfigurable optical add-drop multiplexer (ROADM), channels are added and dropped according to traffic demands and as the result of wavelength routing and lightpath assignment algorithms (RWA).

We introduce the following two definitions. For a given lightpath, channels that are transmitted along the entire lightpath are termed *channels of interest*. However, channels that are added and/or dropped at any point along the lightpath are termed here as *add/drop channels*.

Due to variably loaded network edges, the NLI of the channels of interest is different compared to equivalent point-to-point transmission as different WDM spectra are launched during propagation, emphasizing different XPM contributions $\eta_{XPM}^{(k)}(f_i)$ at each network edges. Additionally, most add/drop channels have already propagated through part of the network,
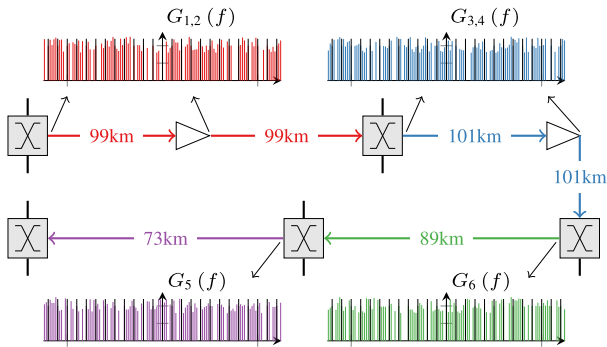
Fig. 7. The lightpath under test, between nodes 15 and 13, from the BT 20+2 topology of the UK core network Fig. 6, showing interfering channels (in color) added and dropped at each ROADM. The channels of interest, that are transmitted along the entire lightpath, are shown in black.

resulting in different amounts of accumulation dispersion compared to a point-to-point transmission.

The analysis is applied to the the British Telecommunications 20+2 topology of the United Kingdom core network [16]. As discussed, for a given network topology and a given traffic demand, a large number of feasible lightpath combinations are possible. For this validation, only one lightpath was analyzed with two different network utilization values. Network utilization is defined as the average spectrum occupancy out of the entire available optical bandwidth.

The lightpath under test is one between node A and B, as shown in Fig. 1. It is assumed that the first two edges, the first edge with 197 km length and the second edge with 203 km length, are each split into two fiber spans. The resulting lightpath of interest is illustrated in Fig. 7, where after each ROADM a different spectrum is launched into the fiber due to the adding and dropping of the add/drop channels. The channels of interest, that are propagated along the entire lightpath, are shown in black and the add/drop channels are shown in color.

For the studied example, several assumptions on the traffic and the established lightpaths are made. Every fifth channel (51 out of a total of 251 channels slots) was a channel of interest and their NLI coefficients were obtained by the SSFM and by the proposed closed-form approximation using (10) and (11). The remaining 200 channel slots were partially filled with add/drop channels which were dropped and added at each ROADM. At each ROADM, 80% of the add/drop channels were randomly dropped and add/drop channels were added by randomly choosing an empty channel slot. The unoccupied channel slots were randomly filled until a certain network utilization value was reached. The considered network utilization values were 80% and 90%.

The added channels exhibit a random power offset between ± 1 dB with respect to the COI to simulate potential non-ideal power equalization. Additionally, this was done in order to test the impact of assumption 3) (see Section II-E) in a network scenario. Add/drop channels were using the same modulation format as the channel under test and were randomly pre-dispersed corresponding to a transmission distance between 0 and 1000 km, to emulate the propagation from different light-

paths in the network. The wavelength dependent gain due to ISRS was ideally compensated after each span to ease a comparison to the point-to-point case in Section III-C.

The NLI coefficient for a network utilization value of 80% is shown in Fig. 8a) and a network utilization of 90% is shown in Fig. 8b). The SSFM results in Fig. 8a) were first published in [14]. The ISRS power transfers were $\Delta\rho(L)\,[\text{dB}] = 5$ dB and $\Delta\rho(L)\,[\text{dB}] = 5.7$ dB, which is less than in the point-to-point case as less average power was launched into a span.

The fluctuating behavior of the NLI coefficient is a direct consequence of the variably loaded network edges. The fluctuations are weaker in the case of 90 % network utilization as a larger average spectral occupation yields more averaging. The change in NLI due to ISRS was -1.6 dB to 1.5 dB for 80% of network utilization and -1.8 dB to 1.6 dB for 90% of network utilization. The proposed closed-form approximation is in good agreement with the simulation results with an average discrepancy of 0.1 dB and 0.2 dB for 80% and 90% network utilization, respectively. Assumption 3) in II-E seems to have a negligible impact on the accuracy of the formula in variably loaded mesh optical networks. The average gap between the closed-form approximation and the SSFM using uniform 64-QAM is 1 dB which is less than in the point-to-point case (cf. Fig. 6) as add/drop channels exhibit, on average, a higher amount of accumulated dispersion.

Based on the validation carried out in this section, it can be concluded that the proposed closed-form approximation models the NLI in mesh optical network scenarios with excellent accuracy. The results in this paper, therefore, enable the performance evaluation of complex light path configurations for an *entire* network topology, within only a few microseconds. This is an essential step in the modeling of optical network performance in the ultra-wideband regime.

IV. NON-UNIFORM (TILTED) LAUNCH POWER DISTRIBUTIONS

In this section, the impact of a tilted launch power distribution on the accuracy of the proposed closed-form is addressed. In the derivation of the proposed closed-form approximation, it is assumed that the effective channel power attenuation is only a function of the total launch power and independent of its spectral distribution (see assumption 3 in Section II-E). The accuracy loss in the case of variable loaded fiber spans was found to be negligible in Section III-D.

The deviation of the SPM contribution using (8) as a function of launch power tilt with respect to a uniform launch power distribution is shown in Fig. 9. A positive launch power tilt means that higher frequency channels have a larger launch power than lower frequency channels.

For a particular launch power tilt, every channel within the WDM signal experiences a slightly different approximation error. Therefore, the average and the maximum deviation over all WDM channels for a given launch power tilt are shown. Fig. 9 shows that the approximation error by considering a uniform launch power compared to a tilted one is fairly small.

However, this approximation error can be completely eliminated with the following approach. The parameters α, $\bar{\alpha}$ and
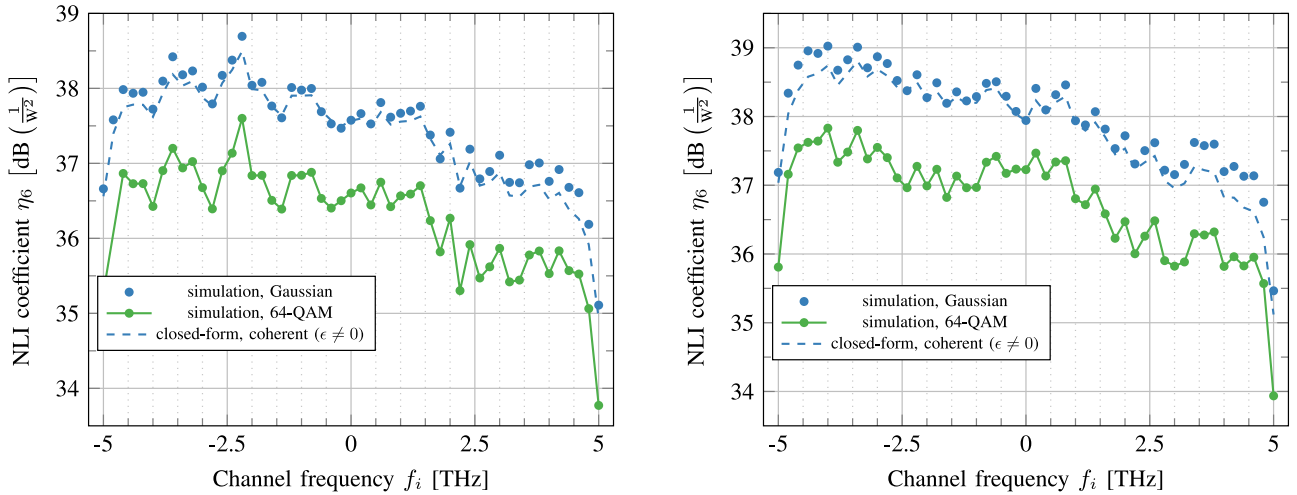
Fig. 8. The NLI coefficient of every fifth channel (i.e. a channel of interest) after six spans where interfering channels are continuously added and dropped along the transmission with a network utilization of 80% shown in a) and 90% shown in b). The results were obtained by numerical simulations and using the proposed closed-form approximation (10) and (11).
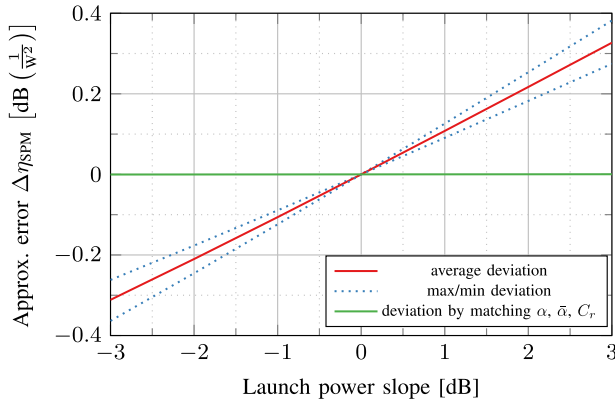

Fig. 9. Approximation error caused by assumption 3) on the SPM contribution using (8). The plot shows the deviation between a tilted launch power distribution and a uniform one as a function of input power slope for a 10.05 THz signal. The average and the maximum deviation of every WDM channel within the signal are shown. Additionally, the deviation is shown by matching α, $\bar{\alpha}$, and C_r to the actual power profile.

C_r in (10) and (11) are reinterpreted as *channel dependent* quantities and matched to the actual power profile of each interfering channel using regression. As shown in Fig. 9, this completely removes the approximation error and fully takes into account the impact of a non-uniform launch power distribution. This shows that assumption 3) can be fully eliminated by matching the parameters α, $\bar{\alpha}$ and C_r to the actual power profile of each interferer. This can be done at the expense of numerically solving the Raman equations and additional regression operations.

V. CONCLUSION

A closed-form approximation of the Gaussian noise model in the presence of inter-channel stimulated Raman scattering was presented.

It was validated using split-step simulations and numerical integrations of the ISRS GN model in integral form, reporting an average deviation of 0.2 dB in nonlinear interference power for SMF based spans operating over the entire C+L band. This discrepancy is primarily because the NLI contribution, that is jointly generated by two interfering channels (FWM or MCI), is neglected and due to the first-order description of ISRS. However, this has little impact for systems with dispersion unmanaged links and high symbol rates or channel spacings. The major discrepancy for the prediction of QAM formats remains the signal Gaussianity assumption, which will be subject of future work.

The results in this paper allow for rapid evaluation of performance (e.g. SNR, maximum reach, optimum launch power) in ultra-wideband transmission systems, an essential step towards dynamic optical network capacity optimization and intelligent information infrastructure design.

APPENDIX A
DERIVATION OF THE XPM CONTRIBUTION

In this section, the closed-form approximation of the XPM contribution (11) is derived. The derivation consists of finding an analytical approximation of the integral form (8) which models the nonlinear interference caused on channel i by a single interfering channel k.

For notational brevity, we define $x(\zeta) = P_{tot}C_r \bar{L}_{eff}(\zeta)$ with $\bar{L}_{eff}(\zeta) = \frac{1-e^{-\bar{\alpha}\zeta}}{\bar{\alpha}}$. To increase the potential parameter space and enable regression approaches, a separate effective length $\bar{L}_{eff}$ is kept in the ISRS term. This allows for a more general application of the proposed formula e.g. in the case of non-uniform (tilted) launch power distributions. Additionally, a pre-factor of $\frac{32}{27}\frac{\gamma^2}{B_k^2}\left(\frac{P_k}{P_i}\right)^2$ is suppressed throughout the derivation. For the ISRS term, the optical power is assumed to be uniformly distributed over the transmitted bandwidth yielding

$\int \frac{1}{P_{\text{tot}}} G_{\text{Tx}}(\nu) e^{-x \cdot \nu} d\nu = \frac{x B_{\text{tot}}}{2 \sinh\left(\frac{x B_{\text{tot}}}{2}\right)}$. Eq. (8) is then written as

$$
\eta_{\text{XPM}}^{(k)}(f_i) = \int_{-\frac{B_i}{2}}^{\frac{B_i}{2}} df_1 \int_{-\frac{B_k}{2}}^{\frac{B_k}{2}} df_2 \, \Pi\left(\frac{f_1 + f_2}{B_k}\right) B_{\text{tot}}
$$

$$
\cdot \left| \int_0^L d\zeta \, \frac{x e^{-\alpha\zeta - x \cdot (f_1 + f_2 + f_i + \Delta f)}}{2 \sinh\left(\frac{x B_{\text{tot}}}{2}\right)} e^{j\phi(f_1 + f_i, f_2 + f_i + \Delta f, f_i, \zeta)} \right|^2
$$

$$
\approx \int_{-\frac{B_i}{2}}^{\frac{B_i}{2}} df_1 \int_{-\frac{B_k}{2}}^{\frac{B_k}{2}} df_2 \, \left| \int_0^L d\zeta \, \frac{x B_{\text{tot}} e^{-\alpha\zeta - x \cdot (f_1 + f_i + \Delta f)}}{2 \sinh\left(\frac{x B_{\text{tot}}}{2}\right)} \right.
$$

$$
\left. \cdot e^{j\phi(f_1 + f_i, f_i + \Delta f, f_i, \zeta)} \right|^2
$$

$$
= 2 B_k \int_0^{\frac{B_i}{2}} df_1 \, \left| \int_0^L d\zeta \, \frac{x B_{\text{tot}} e^{-\alpha\zeta - x \cdot (f_1 + f_i + \Delta f)}}{2 \sinh\left(\frac{x B_{\text{tot}}}{2}\right)} \right.
$$

$$
\left. \cdot e^{j\phi(f_1 + f_i, f_i + \Delta f, f_i, \zeta)} \right|^2, \tag{14}
$$

where $\Delta f = f_k - f_i$ is the (center) frequency separation between channels k and i. In (14), it is assumed that the frequency separation is much larger than half of the bandwidth of channel k (i.e. $|\Delta f| \gg \frac{B_k}{2}$). This assumption allows to approximate $f_2 + \Delta f \approx \Delta f$ and has only a minor accuracy impact on the phase mismatch term ϕ for channels that are close to the COI as addressed in detail in Appendix C. It has negligible impact on the ISRS term (the signal power profile) and the dispersion slope as both are essentially constant over one channel bandwidth B_k. Additionally, the term $\Pi\left(\frac{f_1 + f_2}{B_k}\right)$ was neglected in (14).

For the phase mismatch factor ϕ, we obtain

$$
\phi\left(f_1 + f_i, f_i + \Delta f, f_i, \zeta\right)
$$

$$
= -4\pi^2 f_1 \Delta f \left[\beta_2 + \pi\beta_3(f_1 + 2f_i + \Delta f)\right] \zeta
$$

$$
\approx -4\pi^2 f_1 \Delta f \left[\beta_2 + \pi\beta_3(2f_i + \Delta f)\right] \zeta
$$

$$
= -4\pi^2 f_1 (f_k - f_i) \left[\beta_2 + \pi\beta_3(f_i + f_k)\right] \zeta
$$

$$
= \phi_{i,k} f_1 \zeta, \tag{15}
$$

with $\phi_{i,k} = -4\pi^2 (f_k - f_i) [\beta_2 + \pi\beta_3(f_i + f_k)]$ and where it was assumed that the impact of the dispersion slope is constant over one channel bandwidth B_i. Eq. (15) shows that the XPM assumption and a slowly varying group velocity dispersion, essentially leads to a modification rule of the GVD parameter β_2 to account for the dispersion slope.

In order to simplify (14), the ISRS term is expanded into a Taylor series and truncated to first-order, assuming weak ISRS. The validity range of this approximation is analyzed in Appendix D. Additionally, it is assumed that the signal power profile is constant over one channel bandwidth B_i, mathematically $e^{-x \cdot (f_1 + f_i + \Delta f)} \approx e^{-x \cdot (f_i + \Delta f)} = e^{-x \cdot f_k}$. The Taylor expansion of the ISRS term is then given by

$$
\frac{B_{\text{tot}} x e^{-x \cdot f_k}}{2 \sinh\left(\frac{B_{\text{tot}}}{2} x\right)} = 1 - f_k x + \mathcal{O}(x^2), \tag{16}
$$

and the signal power profile (to first-order) as

$$
\frac{B_{\text{tot}} x e^{-\alpha\zeta - x \cdot f_k}}{2 \sinh\left(\frac{B_{\text{tot}}}{2} x\right)} \approx \left(1 + \tilde{T}_k\right) e^{-\alpha\zeta} - \tilde{T}_k e^{-A\zeta}, \tag{17}
$$

with $\tilde{T}_k = -\frac{P_{\text{tot}} C_{\text{r}}}{\bar{\alpha}} f_k$ and $A = \alpha + \bar{\alpha}$. Enabled by the first-order assumption of ISRS, the following simplification is obtained

$$
\left| \int_0^L d\zeta \, \frac{B_{\text{tot}} x e^{-\alpha\zeta - x \cdot f_k}}{2 \sinh\left(\frac{B_{\text{tot}}}{2} x\right)} e^{j\phi_{i,k} f_1 \zeta} \right|^2
$$

$$
\approx \left| \int_0^L d\zeta \, \left[\left(1 + \tilde{T}_k\right) e^{-\alpha\zeta} - \tilde{T}_k e^{-A\zeta}\right] e^{j\phi_{i,k} f_1 \zeta} \right|^2
$$

$$
\approx \left| -\frac{1 + \tilde{T}_k}{-\alpha + j\phi_{i,k} f_1} + \frac{\tilde{T}_k}{-A + j\phi_{i,k} f_1} \right|^2
$$

$$
= \frac{T_k + \phi_{i,k}^2 f_1^2}{\alpha A^2 + (2\alpha A + \bar{\alpha}^2) \phi_{i,k}^2 f_1^2 + \phi_{i,k}^4 f_1^4}, \tag{18}
$$

where $T_k = (\alpha + \bar{\alpha} - P_{\text{tot}} C_{\text{r}} f_k)^2$ and it was assumed that $e^{-\alpha L} \ll 1$. Substituting the simplification (18) in (14) and using the exact integral identities (29) and (30) yields

$$
2 B_k \int_0^{\frac{B_i}{2}} df_1 \, \left| \int_0^L d\zeta \, \frac{x B_{\text{tot}} e^{-\alpha\zeta - x \cdot f_k}}{2 \sinh\left(\frac{x B_{\text{tot}}}{2}\right)} e^{j\phi_{i,k} f_1 \zeta} \right|^2
$$

$$
\approx \frac{2 B_k}{\phi_{i,k} \bar{\alpha} (2\alpha + \bar{\alpha})} \cdot \left[\frac{T_k - \alpha^2}{\alpha} \text{atan}\left(\frac{\phi_{i,k} B_i}{2\alpha}\right) \right.
$$

$$
\left. + \frac{A^2 - T_k}{A} \, \text{atan}\left(\frac{\phi_{i,k} B_i}{2A}\right)\right]. \tag{19}
$$

In order to obtain the XPM contribution of channel k on channel i, the suppressed pre-factor $\frac{32}{27} \frac{\gamma^2}{B_k^2} \left(\frac{P_k}{P_i}\right)^2$ must be included. Finally, $\phi_{i,k}$ is redefined and the individual XPM contributions $\eta_{\text{XPM}}^{(k)}(f_i)$ are summed up in order to obtain the total XPM contribution $\eta_{\text{XPM}}(f_i)$ as in (11).

APPENDIX B
DERIVATION OF THE SPM CONTRIBUTION

In this section, the closed-form SPM contribution of the NLI (10) is derived. The derivation consists of finding an analytical approximation of the integral expression (8) which models the nonlinear interference caused by channel i on itself. The reader is reminded that, for the SPM contribution, a factor of $\frac{1}{2}$ must be multiplied to (8). For notational brevity, we define $x(\zeta) = P_{\text{tot}} C_{\text{r}} \bar{L}_{\text{eff}}(\zeta)$ with $\bar{L}_{\text{eff}}(\zeta) = \frac{1 - e^{-\bar{\alpha}\zeta}}{\bar{\alpha}}$ and a pre-factor of $\frac{16}{27} \frac{\gamma^2}{B_i^2}$ is suppressed throughout the derivation.

The NLI coefficient of the SPM contribution is then written as

$$\eta_{\text{SPM}}(f_i) \approx \int_{-\frac{B_i}{2}}^{\frac{B_i}{2}} df_1 \int_{-\frac{B_i}{2}}^{\frac{B_i}{2}} df_2$$

$$\cdot \left| \int_0^L d\zeta \, \frac{x B_{\text{tot}} e^{-\alpha\zeta - x f_i}}{2\sinh\left(\frac{x B_{\text{tot}}}{2}\right)} e^{j\phi(f_1+f_i,f_2+f_i,f_i,\zeta)} \right|^2$$

$$\approx \int_{-\frac{B_i}{2}}^{\frac{B_i}{2}} df_1 \int_{-\frac{B_i}{2}}^{\frac{B_i}{2}} df_2 \, \frac{T_i + \phi_i^2 f_1^2 f_2^2}{\alpha A^2 + \left(2\alpha A + \bar{\alpha}^2\right)\phi_i^2 f_1^2 f_2^2 + \phi_i^4 f_1^4 f_2^2}, \tag{20}$$

with $\phi_i = -4\pi^2\left(\beta_2 + 2\pi\beta_3 f_i\right)$ and where the first-order description of ISRS was used and it was assumed that the signal power profile and the dispersion slope are constant over one channel bandwidth B_i (see Appendix A).

Eq. (20) can be solved exactly in terms of elementary functions over a closed circular integration domain. The radius of the circular domain is chosen such that its area equals that of the actual integration domain, as proposed in [20]. The actual integration domain and its approximated circular domain are shown as insets in Fig. 3. Exploiting the circular domain approximation, Eq. (20) is recast in polar coordinates and solved using the integral identities (31) and (32) as

$$\eta_{\text{SPM}}(f_i) \approx 4 \int_0^{\sqrt{\frac{3}{\pi}}\frac{B_i}{2}} dr \int_0^{\frac{\pi}{2}} d\phi$$

$$\frac{r T_i + \frac{\phi_i^2}{4} r^5 \sin^2(\phi)}{\alpha A^2 + \frac{\phi_i^2}{4}\left(2\alpha A + \bar{\alpha}^2\right) r^4 \sin^2(\phi) + \frac{\phi_i^4}{16} r^8 \sin^4(\phi)}$$

$$= \int_0^{\sqrt{\frac{3}{\pi}}\frac{B_i}{2}} dr \, \frac{4\pi}{\bar{\alpha}\left(2\alpha + \bar{\alpha}\right)}$$

$$\cdot \left(\frac{T_i - \alpha^2}{\alpha^2} \frac{r}{\sqrt{1 + \frac{\phi_i^2}{4\alpha^2} r^4}} + \frac{A^2 - T_i}{A^2} \frac{r}{\sqrt{1 + \frac{\phi_i^2}{4A^2} r^4}} \right)$$

$$= \frac{2\pi}{\phi_i \bar{\alpha}\left(2\alpha + \bar{\alpha}\right)}$$

$$\cdot \left[\frac{T_i - \alpha^2}{a} \text{asinh}\left(\frac{3\phi_i B_i^2}{8\pi a}\right) + \frac{A^2 - T_i}{A} \text{asinh}\left(\frac{3\phi_i B_i^2}{8\pi A}\right) \right] \tag{21}$$

In order to obtain the SPM contribution, the suppressed pre-factor $\frac{16}{27}\frac{\gamma^2}{B_i^2}$ must be included and ϕ_i is redefined in order to obtain (10).

APPENDIX C
ADDRESSING ASSUMPTION 1)

In this section, the assumption 1) in Section II-E is addressed in more detail. Assumption 1) states that the channel separation between COI and INT has to be much greater than half of the channel bandwidth $|\Delta f| \gg \frac{B_k}{2}$. To mathematically quantify the impact of the assumption we start with the XPM contribution as in (8). For simplification, ISRS is neglected and

$\tilde{\phi}_{i,k} = -4\pi^2\left[\beta_2 + \pi\beta_3(f_i + f_k)\right]$ similar to Appendix A. For notational brevity, the pre-factor $\frac{32}{27}\frac{\gamma^2}{B_k^2}\left(\frac{P_k}{P_i}\right)^2$ is not shown, as it does not alter the analysis in this section. The NLI coefficient is then given as

$$\tilde{\eta}_{\text{XPM}}^{(k)}(f_i) = \int_0^{\frac{B_i}{2}} df_1 \int_{-\frac{B_k}{2\Delta f}}^{\frac{B_k}{2\Delta f}} df_2 \, \frac{2\Delta f}{\alpha^2} \frac{1}{1 + \tilde{\mu} f_1^2 \left(f_2 + 1\right)^2}, \tag{22}$$

with $\tilde{\mu} = \frac{\tilde{\phi}_{i,k}^2 \Delta f^2}{\alpha^2}$ and where it was assumed that $e^{-\alpha L} \ll 1$ and $\Pi\left(\frac{f_1 + f_2}{B_k}\right)$ was neglected as in Appendix A.

As the channel spacing is at least $\Delta f > \frac{B_k}{2}$, the inner integration variable in (22) varies as $f_2 \in [-1,1]$. Therefore, the integrand in (22) is expanded into a converging Taylor series and truncated after second-order

$$\int_{-\frac{B_k}{2\Delta f}}^{\frac{B_k}{2\Delta f}} df_2 \, \frac{2\Delta f}{1 + \tilde{\mu} f_1^2 \left(f_2 + 1\right)^2} \approx$$

$$\underbrace{\frac{2B_k}{\tilde{\mu} f_1^2 + 1}}_{\text{zeroth-order}} + \underbrace{\frac{\tilde{\mu} f_1^2 \left(3\tilde{\mu} f_1^2 - 1\right) B_k^2}{6\Delta f^2 \left(\tilde{\mu} f_1^2 + 1\right)^3}}_{\text{second-order}}, \tag{23}$$

where the first-order term yields zero after integration. Mathematically, the assumption $|f_k - f_i| = |\Delta f| \gg \frac{B_k}{2}$ (or simply $f_2 = 0$) in II-C *coincides* with the zeroth-order approximation of the integral over the variable f_2. The relative error can be therefore obtained by analyzing the higher-order terms. Inserting the Taylor approximation (23) in (22) and solving the integrals using (33) and (34) yields

$$\tilde{\eta}_{\text{XPM}}^{(k)}(f_i) \approx \frac{B_k B_i}{\alpha^2 \mu}$$

$$\cdot \left\{ \underbrace{\text{atan}(\mu)}_{\text{zeroth-order}} + \underbrace{\frac{B_k^2}{12\Delta f^2}\left[\text{atan}(\mu) - \frac{\mu\left(2\mu^2 + 1\right)}{\left(\mu^2 + 1\right)^2}\right]}_{\text{second-order}} \right\}, \tag{24}$$

with $\mu = \frac{|\tilde{\phi}_{i,k}||\Delta f| B_i}{2\alpha}$. The zeroth-order term in (24) is identical to the proposed closed-form (10) in the absence of ISRS. Finally, the relative error, caused by Assumption 1) in Section II-E is obtained by normalizing the second-order term by the zeroth-order term. Therefore, the relative error is given by

$$\text{Rel. Err.} = \frac{1}{12}\frac{B_k^2}{\Delta f^2}\left[1 - \frac{\mu\left(2\mu^2 + 1\right)}{\left(\mu^2 + 1\right)^2 \text{atan}(\mu)}\right] < \frac{1}{12}\frac{B_k^2}{\Delta f^2}. \tag{25}$$

Eq. (25) can be reliably used to quantify the approximation error caused by Assumption 1).

APPENDIX D
DERIVATION OF THE VALIDITY RANGE

In order to derive a validity range of the weak ISRS assumption, the ISRS term to first-order is compared to the ISRS term to second-order at a frequency component f_k. The first-order

approximation is then valid when the second-order term is negligible. The second coefficient of the Taylor series, as in (16), is given by

$$\tilde{T}_k^{(2)} = \frac{f_k^2}{2} - \frac{B^2}{24}. \tag{26}$$

Requiring that the second-order term is negligible to the first-order approximation yields

$$|f_k x| \gg \left| \tilde{T}_k^{(2)} x^2 \right| = \left| \frac{f_k^2}{2} - \frac{B_{\text{tot}}^2}{24} \right| x^2. \tag{27}$$

The channel that is most impacted by ISRS is the channel with center frequency $f_k = \frac{B}{2}$ for which we will evaluate (27) and obtain

$$B_{\text{tot}} P_{\text{tot}} L_{\text{eff}} C_r = 0.23 \cdot \Delta\rho(L)\,[\text{dB}] \ll 6, \tag{28}$$

where $\Delta\rho(L)\,[\text{dB}]$ is the ISRS power transfer between the outer channels of the transmitted signals as in Eq. (3).

APPENDIX E
INTEGRAL IDENTITIES

This section contains the integral identities that were used in order to derive the proposed closed-form expression.

$$\int_0^X dx\, \frac{1}{a + bx^2 + x^4}$$
$$= \frac{\sqrt{2}}{a\sqrt{b-c}}\text{atan}\left(\frac{\sqrt{2}X}{\sqrt{b-c}}\right) - \frac{\sqrt{2}}{C\sqrt{b+c}}\text{atan}\left(\frac{\sqrt{2}X}{\sqrt{b+c}}\right), \tag{29}$$

$$\int_0^X dx\, \frac{x^2}{a + bx^2 + x^4}$$
$$= \frac{\sqrt{b+c}}{\sqrt{2}c}\,\text{atan}\left(\frac{\sqrt{2}X}{\sqrt{b+c}}\right) - \frac{\sqrt{b-c}}{\sqrt{2}c}\,\text{atan}\left(\frac{\sqrt{2}X}{\sqrt{b-c}}\right), \tag{30}$$

with $c = \sqrt{b^2 - 4a}$.

$$\int_0^{\frac{\pi}{2}} dx\, \frac{1 + a\sin^2(x)}{1 + b\sin^2(x) + c\sin^4(x)}$$
$$= \frac{\pi}{\sqrt{(2)}\tilde{a}}\left\{ j\frac{[a(\tilde{a} - c) + 2c]}{\tilde{b}} + \frac{[a(\tilde{a} + c) - 2c]}{\tilde{c}} \right\}, \tag{31}$$

where $\tilde{a} = \sqrt{b^2 - 4c}$, $\tilde{b} = \sqrt{b(A - b) + c(A - b + 2)}$, $\tilde{c} = \sqrt{b(A + b) + c(A + b - 2)}$ and $j = \sqrt{-1}$.

$$\int_0^X \frac{1}{\sqrt{1 + a^2 x^4}} = \frac{1}{2a}\text{asinh}\left(aX^2\right) \tag{32}$$

$$\int_0^X \frac{1}{a^2 x^2 + 1}dx = \frac{\text{atan}(aX)}{a}, \tag{33}$$

$$\int_0^X \frac{x^2\left(3a^2 x^2 - 1\right)}{\left(a^2 x^2 + 1\right)^3}dx = \frac{\text{atan}(aX)}{a^3} - \frac{X\left(2a^2 X^2 + 1\right)}{a^2\left(a^2 X^2 + 1\right)^2}. \tag{34}$$

REFERENCES

[1] T. Hasegawa, Y. Yamamoto, and M. Hirano, "Optimal fiber design for large capacity long haul coherent transmission," *Opt. Express*, vol. 25, no. 2, pp. 706–712, Jan. 2017.

[2] D. Semrau *et al.*, "Achievable information rates estimates in optically amplified transmission systems using nonlinearity compensation and probabilistic shaping," *Opt. Lett.*, vol. 42, no. 1, pp. 121–124, Dec. 2016.

[3] G. Bosco, P. Poggiolini, A. Carena, V. Curri, and F. Forghieri, "Analytical results on channel capacity in uncompensated optical links with coherent detection," *Opt. Express*, vol. 19, no. 26, pp. B440–B451, Dec. 2011.

[4] N. A. Shevchenko *et al.*, "Achievable information rates estimation for 100-nm Raman-amplified optical transmission system," in *Proc. 42nd Eur. Conf. Opt. Commun.*, 2016, pp. 1–3.

[5] V. Anagnostopoulos, C. T. Politi, C. Matrakidis, and A. Stavdas, "Physical layer impairment aware wavelength routing algorithms based on analytically calculated constraints," *Opt. Commun.*, vol. 270, no. 2, pp. 247–254, Feb. 2007.

[6] A. Nespola *et al.*, "GN-model validation over seven fiber types in uncompensated PM-16QAM Nyquist-WDM links," *IEEE Photon. Technol. Lett.*, vol. 26, no. 2, pp. 206–209, Jan. 2014.

[7] A. Nespola *et al.*, "Experimental validation of the EGN-model in uncompensated optical links," in *Proc. Opt. Fiber Commun. Conf.*, 2015, pp. 1–3.

[8] L. Galdino *et al.*, "Experimental demonstration of modulation-dependent nonlinear interference in optical fibre communication," in *Proc. 42nd Eur. Conf. Opt. Commun.*, 2016, pp. 1–3.

[9] G. Saavedra *et al.*, "Experimental investigation of nonlinear signal distortions in ultra-wideband transmission systems," in *Proc. Opt. Fiber Commun. Conf. Exhib.*, 2017, pp. 1–3.

[10] G. Saavedra *et al.*, "Experimental analysis of nonlinear impairments in fibre optic transmission systems up to 7.3 THz," *J. Lightw. Technol.*, vol. 35, no. 21, pp. 4809–4816, Nov. 2017.

[11] G. Saavedra *et al.*, "Inter-channel stimulated Raman scattering and its impact in wideband transmission systems," in *Proc. Opt. Fiber Commun. Conf.*, 2018, pp. 1–3.

[12] J. Tang, "The channel capacity of a multispan DWDM system employing dispersive nonlinear optical fibers and an ideal coherent optical receiver," *J. Lightw. Technol.*, vol. 20, no. 7, pp. 1095–1101, Jul. 2002.

[13] P. Poggiolini, "The GN model of non-linear propagation in uncompensated coherent optical systems," *J. Lightw. Technol.*, vol. 30, no. 24, pp. 3857–3879, Dec. 2012.

[14] D. Semrau, E. Sillekens, R. I. Killey, and P. Bayvel, "The ISRS GN model, an efficient tool in modeling ultra-wideband transmission in point-to-point and network scenarios," in *Proc. Eur. Conf. Opt. Commun.*, 2018, pp. 1–3.

[15] M. Cantono *et al.*, "On the interplay of nonlinear interference generation with stimulated Raman scattering for QoT estimation," *J. Lightw. Technol.*, vol. 36, no. 15, pp. 3131–3141, Aug. 2018.

[16] D. J. Ives, A. Lord, P. Wright, and S. J. Savory, "Quantifying the impact of non-linear impairments on blocking load in elastic optical networks," in *Proc. Opt. Fiber Commun. Conf.*, 2014, pp. 1–5.

[17] A. Splett, C. Kurtzke, and K. Petermann, "Ultimate transmission capacity of amplified optical fiber communication systems taking into account fiber nonlinearities," in *Proc. Eur. Conf. Opt. Commun.*, 1993, pp. 41–44.

[18] H. Louchet, A. Hodzic, and K. Petermann, "Analytical model for the performance evaluation of DWDM transmission systems," *IEEE Photon. Technol. Lett.*, vol. 15, no. 9, pp. 1219–1221, Sep. 2003.

[19] X. Chen and W. Shieh, "Closed-form expressions for nonlinear transmission performance of densely spaced coherent optical OFDM systems," *Opt. Express*, vol. 18, no. 18, pp. 19039–19054, Aug. 2010.

[20] S. J. Savory, "Approximations for the nonlinear self-channel interference of channels with rectangular spectra," *IEEE Photon. Technol. Lett.*, vol. 25, no. 10, pp. 961–964, May 2013.

[21] P. Johannisson and E. Agrell, "Modeling of nonlinear signal distortion in fiber-optic networks," *J. Lightw. Technol.*, vol. 32, no. 23, pp. 3942–3950, Dec. 2014.

[22] P. Poggiolini, G. Bosco, A. Carena, V. Curri, Y. Jiang, and F. Forghieri, "A simple and effective closed-form GN model correction formula accounting for signal non-Gaussian distribution," *J. Lightw. Technol.*, vol. 33, no. 2, pp. 459–473, Jan. 2015.

[23] D. Semrau, G. Saavedra, D. Lavery, R. I. Killey, and P. Bayvel, "A closed-form expression to evaluate nonlinear interference in Raman-amplified links," *J. Lightw. Technol.*, vol. 35, no. 19, pp. 4316–4328, Oct. 2017.

[24] D. Semrau, R. Killey, and P. Bayvel, "Achievable rate degradation of ultra-wideband coherent fiber communication systems due to stimulated Raman scattering," *Opt. Express*, vol. 25, no. 12, pp. 13024–13034, Jun. 2017.

[25] I. Roberts, J. M. Kahn, J. Harley, and D. W. Boertjes, "Channel power optimization of WDM systems following Gaussian noise nonlinearity model in presence of stimulated Raman scattering," *J. Lightw. Technol.*, vol. 35, no. 23, pp. 5237–5249, Dec. 2017.

[26] M. Cantono, J. L. Auge, and V. Curri, "Modelling the impact of SRS on NLI generation in commercial equipment: An experimental investigation," in *Proc. Opt. Fiber Commun. Conf. Expo.*, 2018, pp. 1–3.

[27] D. Semrau, R. I. Killey, and P. Bayvel, "The Gaussian Noise model in the presence of inter-channel stimulated Raman scattering," *J. Lightw. Technol.*, vol. 36, no. 14, pp. 3046–3055, Jul. 2018.

[28] D. Semrau, R. I. Killey, and P. Bayvel, "A closed-form approximation of the Gaussian Noise model in the presence of inter-channel stimulated Raman scattering," 2018, arXiv:1808.07940.

[29] P. Poggiolini, "A generalized GN-model closed-form formula," 2018, arXiv:1810.06545v2.

[30] R. H. Stolen and E. P. Ippen, "Raman gain in glass optical waveguides," *App. Phys. Lett.*, vol. 22, no. 6, pp. 276–278, 1973.

[31] F. Forghieri, R. W. Tkach, and A. R. Chraplyvy, "Effect of modulation statistics on Raman crosstalk in WDM systems," *IEEE Photon. Technol. Lett.*, vol. 7, no. 1, pp. 101–103, Jan. 1995.

[32] K.-P. Ho, "Statistical properties of stimulated Raman crosstalk in WDM systems," *J. Lightw. Technol.*, vol. 18, no. 7, pp. 915–921, Jul. 2000.

[33] K. Minoguchi *et al.*, "Experiments on stimulated Raman scattering in S- and L-bands 16-QAM signals for ultra-wideband coherent WDM systems," in *Proc. Opt. Fiber Commun. Conf. Expo.*, 2018, pp. 1–3.

[34] D. N. Christodoulides and R. B. Jander, "Evolution of stimulated Raman crosstalk in wavelength division multiplexed systems," *IEEE Photon. Technol. Lett.*, vol. 8, no. 12, pp. 1722–1724, Dec. 1996.

[35] M. Zirngibl, "Analytical model of Raman gain effects in massive wavelength division multiplexed transmission systems," *Electron. Lett.*, vol. 34, no. 8, pp. 789–790, Apr. 1998.

[36] A. Mecozzi and R.-J. Essiambre, "Nonlinear shannon limit in pseudolinear coherent systems," *J. Lightw. Technol.*, vol. 30, no. 12, pp. 2011–2024, Jun. 2012.

[37] M. Secondini and E. Forestieri, "Analytical fiber-optic channel model in the presence of cross-phase modulation," *IEEE Photon. Technol. Lett.*, vol. 24, no. 22, pp. 2016–2019, Nov. 2012.

[38] R. Dar, M. Feder, A. Mecozzi, and M. Shtaif, "Properties of nonlinear noise in long, dispersion-uncompensated fiber links," *Opt. Express*, vol. 21, no. 22, pp. 25685–25699, Oct. 2013.

[39] D. J. Ives, P. Bayvel, and S. J. Savory, "Adapting transmitter power and modulation format to improve optical network performance utilizing the Gaussian noise model of nonlinear impairments," *J. Lightw. Technol.*, vol. 32, no. 21, pp. 4087–4096, Nov. 2014.

[40] A. Carena, G. Bosco, V. Curri, Y. Jiang, P. Poggiolini, and F. Forghieri, "EGN model of non-linear fiber propagation," *Opt. Express*, vol. 22, no. 13, p. 16335, Jun. 2014.

[41] F. Zhang, Q. Zhuge, and D. V. Plant, "Fast analytical evaluation of fiber nonlinear noise variance in mesh optical networks," *IEEE/OSA J. Opt. Commun. Netw.*, vol. 9, no. 4, pp. C88–C97, Apr. 2017.

[42] D. J. Ives, A. Alvarado, and S. J. Savory, "Adaptive transceivers in nonlinear flexible networks," in *Proc. 42nd Eur. Conf. Opt. Commun.*, Sep. 2016, pp. 1–3.

[43] D. Semrau, E. Sillekens, R. I. Killey, and P. Bayvel, "ISRS GN model implementation," 2019. [Online]. Available: https://github.com/dsemrau/ISRSGNmodel

[44] G. Forney, R. Gallager, G. Lang, F. Longstaff, and S. Qureshi, "Efficient modulation for band-limited channels," *IEEE J. Sel. Areas Commun.*, vol. 2, no. 5, pp. 632–647, Sep. 1984.

[45] T. Fehenberger, A. Alvarado, G. Böcherer, and N. Hanik, "On probabilistic shaping of quadrature amplitude modulation for the nonlinear fiber channel," *J. Lightw. Technol.*, vol. 34, no. 21, pp. 5063–5073, Nov. 2016.

Daniel Semrau (S'16) received the B.Sc. degree in electrical engineering from the Technical University of Berlin, Berlin, Germany, in 2013, and the M.Sc. degree in photonic networks engineering from Scuola Superiore SantAnna, Pisa, Italy, and Aston University, Birmingham, U.K., in 2015. In 2015, he joined the Optical Networks Group, University College London, U.K., where he is currently working toward the Ph.D. degree. His research interests are mainly focused on channel modeling, nonlinear compensation techniques, and ultra-wideband transmission coherent optical communications. He was the recipient of the Graduate Student Fellowship award of the IEEE Photonics Society in 2018.

Robert I. Killey (SM'17) received the B.Eng. degree in electronic and communications engineering from the University of Bristol, Bristol, U.K., in 1992, the M.Sc. degree from University College London (UCL), London, U.K., in 1994, and the D.Phil. degree from the University of Oxford, Oxford, U.K., in 1998. He is currently an Associate Professor with the Optical Networks Group with UCL, London, U.K. and a Principal Investigator in the EPSRC funded UNLOC project. His research interests include nonlinear fiber effects in WDM transmission, advanced modulation formats, and digital signal processing for optical communications. He has participated in many European projects, including ePhoton/ONe, Nobel, BONE and ASTRON, and national projects. He was with the Technical Program Committees of many international conferences including European Conference on Optical Communication, Optical Fiber Communication Conference ACP, and OECC. He was an Associate Editor of the IEEE/OSA JOURNAL OF OPTICAL COMMUNICATIONS AND NETWORKING and is currently an Associate Editor of the JOURNAL OF LIGHTWAVE TECHNOLOGY.

Polina Bayvel (F'10) received the B.Sc.(Eng.) and Ph.D. degrees in electronic and electrical engineering from the University of London (UCL), London in 1986 and 1990, respectively. In 1990, she was with the Fiber Optics Laboratory, General Physics Institute, Moscow, Russian Academy of Sciences, under the Royal Society Postdoctoral Exchange Fellowship. She was a Principal Systems Engineer with STC Submarine Systems, Ltd., London, U.K., and Nortel Networks (Harlow, U.K., and Ottawa, ON, Canada), where she was involved in the design and planning of optical fibre transmission networks. During 1994–2004, she held a Royal Society University Research Fellowship at University College London (UCL), London, U.K., where she became a Chair in Optical Communications and Networks. She is currently the Head of the Optical Networks Group, UCL, which she set up in 1994. She has authored or coauthored more than 300 refereed journal and conference papers. She leads the UK EPSRC Programme TRANSNET (2018–2024). Her research interests include wavelength-routed optical networks, high-speed optical transmission, and the study and mitigation of fibre nonlinearities. She is a Fellow of the Royal Academy of Engineering, the Optical Society of America and the U.K. Institute of Physics. She is an Honorary Fellow of the Institution of Engineering and Technology (FIET). She was a recipient of the Royal Society Wolfson Research Merit Award (2007–2012), the 2013 IEEE Photonics Society Engineering Achievement Award, the 2014 Royal Society Clifford Patterson Prize Lecture and Medal, and the 2015 Royal Academy of Engineering Colin Campbell Mitchell Award.